The Meyer-Neldel Rule in Layered Silicone-Silver Nanocomposites

A. Yildiz,[1] F. Iacomi,[2] M. Cazacu,[3] A. Amironesei,[2] G.I. Rusu,[2] S. Simon[4,5]
[1]*Department of Physics, Faculty of Science and Arts, Ahi Evran University, 40040 Kirsehir, Turkey*

[2]*Department of Physics, Faculty of Physics, Alexandru Ioan Cuza University, 11 Carol I Blvd., 700506 Iasi, Romania*

[3]*Institute of Macromolecular Chemistry 'Petru Poni', Aleea Grigore Ghica Voda, nr. 41A, 700487 Iasi, Romania*

[4]*Department of Material Physics and Advanced Technologies, Faculty of Physics, Babes Bolyai University, 1 M. Kogalniceanu Street, 3400 Cluj-Napoca, Romania*

[5]*Interdisciplinary Research Institute in Bio-Nano-Sciences, Babes Bolyai University, 1 M. Kogalniceanu Street, 3400 Cluj-Napoca, Romania*

X-Ray diffraction and X-ray photoelectron spectroscopy studies, applied on some silicone-silver nanocomposites, revealed the influence of the solvent used in preparation on the morphology of the resulted materials. It has been emphasized that dimethylformamide solvent favors the formation of silver nanoparticles and their migration at the surface, while water solvent favors the formation of a homogeneous composite with small silver nanoparticles. The places occupied by Ag nanoparticles (some prevent their oxidation and others that favor the oxidation process) are dependent on the mixture used in sol-gel technique and have influence on the nanocomposite electrical conductivity. The temperature dependence of the electrical conductivity is investigated. A linear relationship between the pre-exponential factor (σ_0) and activation energy (E_a) was observed, in the high temperature range ($T > 315$ K), for all the samples, indicating that the conductivity data obey Meyer-Neldel rule. POLYM. COMPOS., 32:1751–1756, 2011. © 2011 Society of Plastics Engineers

INTRODUCTION

Polymer/metal nanocomposites and particularly polymer/silver composites with well-defined dimensions and structures are of particular interest due to their specific catalytic, antimicrobial, optical, electronic, and magnetic properties [1–4].

The sol-gel technique, consisting in hydrolysis and condensation reactions of the matrix precursor, has attracted much interest for preparing nanocomposites containing metallic nanoparticles because it can be controlled at mild and biocompatible conditions [5, 6].

In a previous article [7], we reported the preparation of silicone-silver composites containing in situ generated silver nanoparticles.

By using X-ray diffraction (XRD), scanning electron microscopy, optical spectroscopy, and electron paramagnetic resonance methods, it was evidenced that dimethylformamide (DMF) solutions and low water contents favor the formation of silver aggregates on the of upper surface of the layer and that high water content favors the formation of a homogeneous composite containing small silver nanoparticles [7, 8].

It was established that the electrical conductivity of silver-polymer composites was enhanced by increasing the silver amount, whereas the flexibility was achieved by decreasing it [7, 9]. On the other hand, for a composite with narrower size distribution of conducting fillers or monosize distribution as an extreme case, less number of direct contacts between fillers are expected, contributing to higher composite resistivity.

In our experimental results, there was an uncertainty concerning the influence of the chemical state of nanoparticles on the nature of the electron transport in nanocomposites. To provide a better understanding of temperature-

Correspondence to: F. Iacomi; e-mail: f_iacomi@yahoo.com
Contract grant sponsor: ELOTRANSP (PN II-PC); contract grant number: 12-128/2008.
DOI 10.1002/pc.21204
Published online in Wiley Online Library (wileyonlinelibrary.com).

dependent conductivity, a more detailed analysis is needed. On the other hand, there are only few attempts to explain electrical conduction mechanism in nanocomposites to date [10, 11]. To overcome the lack of studies explaining the electrical conduction in nanocomposites, it is necessary to correctly determine kinds of electrical conduction mechanism.

To give a rational explanation about the influence of nature of nanoparticles on the electron transport in silicone-silver composites, XRD and X-ray photoelectron spectroscopy (XPS) are used to examine the structure and bonding structure, while Meyer-Neldel rule (MNR) is used to describe the temperature dependent conductivity.

EXPERIMENTAL

Three composites, C1, C2, and C3 were prepared as already was described in Ref. 7 by mixing methyltrimethoxysilane (MTES), dimethyldiethoxysilane (DMDES), and 3-aminopropyltriethoxysilane (APTES), after which silver nitrate was added dissolved either in DMF-water mixture or in water only in the ratios presented in Table 1. Each of the three prehydrolyzed silanes were introduced to fulfill a certain role. While DMDES is a precursor for highly flexible dimethylsiloxane chain, MTES is a crosslinker highly compatible with polydimethylsiloxane and APTES is a particle stabilizer, as it can readily complex to metal through its amine functionality.

The obtained sols were layered on glass substrates and aged in the laboratory environment when yellowish to brown films were formed. Layer thicknesses, d, were determined by mean of a DEKTAK profilometer. Silver contents (at%) and Ag/Si ratios were evaluated from the energy dispersive X-ray spectra (EDX), registrated for the cross section and the upper surface of composite layers, respectively (VEGA II LSH with EDX - QUANTAX QX). The determined values are shown in Table 1 [7, 8].

The silver-composite layers were structurally analyzed by using a Shimadzu LabX XRD-6000 equipment (standard XRD technique with CuK_α radiation, $\lambda = 1.5418$ Å). Silver particle sizes, D, were determined from Scherrer's equation [7].

Compositional analysis and binding energies of the film surface was conducted using XPS (XPS SPECS PHOIBOS 150 MCD, Al K_α source, 1486.6 eV). Charge referencing was used for all spectra by applying charge correction to the saturated hydrocarbon C 1s peak at the binding energy of 284.6 eV. Analysis of the spectra was performed by using XPSPEAK4.1 fitting program. This analysis typically involved back-ground subtraction using the Shirley method followed by nonlinear least squares fitting to a mixed Gaussian–Lorentzian peak shape. Although the algorithm used requires the user to define initial conditions for the fitting procedure, we typically explored several different curve-fitting procedures to determine the sensitivity of the results to the fitting procedure, using the results to estimate uncertainty in both peak position and area.

Electrical properties of silicone-silver composites were investigated as a function of temperature, in a two-point probe arrangement, using a Keithley 6517A Electometer. The electrical conductivities were determined by measuring the volume electrical resistance, under normal air atmosphere. The MNR is used to describe the high temperature conductivity data of the samples.

RESULTS AND DISCUSSION

The XRD patterns of composites are shown in Fig. 1a. A broad peak centered at $2\theta = 23^\circ$ is observed for all samples and can be ascribed to weak ordering parallel to the polymer chain. Sharp XRD peaks corresponding to (111), (200), (220), and (311) silver planes are evidenced for sample C1. As expected, the intensity of the Ag diffraction peaks increases significantly with the feed amount of $AgNO_3$. These results indicate that the Ag (I) complex ions in the silicone-silver films were reduced to form Ag metal crystals. All the peaks can be indexed to face-centered cubic silver belonging to space group Fm3m (no. 225). The silver was preferentially oriented along the (111) plane. XRD patterns of samples C2 and C3 do not show sharp XRD peaks in agreement with the previous results [7]. These results evidence the role of DMF in Ag (I) complex ion reduction.

A decomposition of (111) XRD peak in two Gaussian components, I_1 and I_2 (Fig. 1a) was performed, and the results are presented in Table 2. Lattice parameters as determined from (111) XRD peak evidence a linear dependence on the particle radius reciprocal, conform to the literature [9]. The ratio of intensities of (111) XRD peak components, I_1/I_2, is dependent on DMF content in the reaction medium, decreasing from the value of 2.6 for sample C1 to the value of 1.4 for sample C2.

To get more information about chemical state of silver nanoparticles, XPS investigations were performed. Figure 2 shows the wide scan XPS spectra of the upper surface

TABLE 1. The molar composition of the mixtures used for the composites preparation. Silver contents and thickness of composite layers [7].

	Feed molar parts								
Sample	MTES	DMDES	APTES	H_2O	DMF	$AgNO_3$	Ag (at%)	Ag/Si surface	D (μm)
C1	1	1	1.5	9.5	1.7	1.0	4.80	2.06	36.6
C2	1	1	2.0	11.0	1.8	0.8	3.50	0.20	35.7
C3	1	1	1.5	17.4	–	0.8	3.68	0.21	36.3

DOI 10.1002/pc

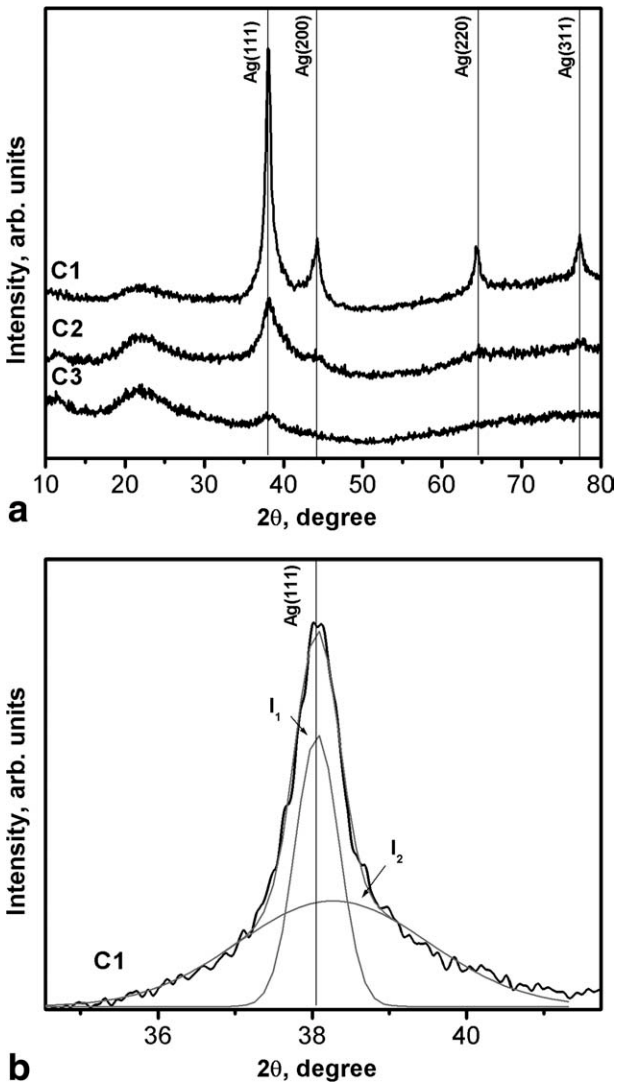

FIG. 1. (a) XRD patterns of layered silicone-silver composites; (b) Decomposition of (111) XRD peak in its Gaussian components.

of C1, C2, and C3 silicone-silver composites. The binding energies of the Si 2p, C 1s, Ag 3d, N 1s, and O1s electron levels are close to those reported in the literature [9–12]. Some differences in the intensities of these XPS peaks are evident. XPS peaks of Ag 3d observed in the XPS survey of sample C1 are more intense than those observed in XPS spectra of sample C2 and C3. This result can be related to the silver nanoparticles migrated at the film surface, nanoparticles evidenced also by our previous SEM analysis [7]. The presence of Ag nanoparticles at the film surface explain also why the XPS peaks of Si 2p are less intense in comparison with those observed in the survey spectra of sample C2 and C3.

Two bands are visible in the XPS spectrum of sample C1 located at about 374.4 and 368.4 eV, corresponding to the binding energies of $3d_{3/2}$ and $3d_{5/2}$ of silver, respectively (Fig. 3a). According to the literature, the location of the XPS peaks of silver depends on the chemical state of the silver element and the size of the nanoparticles [12–15]. The size effect is due to the change in electronic structure that results from changes in the boundary conditions with changes in size of the nanoparticles. When water is present in the reaction medium, micellization can occur due to the coexistence of hydrophobic dimethylsiloxane moiety and hydrophilic NH_2 group leading to the formation and stabilization of the small particles.

The chemical effect on the binding energy is due to the adsorption of polymer onto the nanoparticles. Both these effects are evidenced in the XPS spectra of sample C2 and C3, not only for Ag 3d but also for O1s and N1s (Fig. 3b and c, Table 2). As is shown in Scheme 1, both primary and secondary carbon atoms can be found in the sample. NH_2 group can exist as free or involved in silver coordination. At the same time, Ag can bind oxygen from Si-OH groups by either coordination or covalent bonds. XPS analysis indicates places that prevent Ag nanoparticles from being oxidized and others that favor the oxidation process.

Table 2 shows strong differences in the percentage of chemical states of Si 2p and C1s at the surface of samples C2 and C3 which may influence the samples properties.

At room temperature, the electrical conductivity values of composite layers are: 8.03×10^{-7} $(\Omega\ \text{cm})^{-1}$ (sample C1), 4.26×10^{-7} $(\Omega\ \text{cm})^{-1}$ (sample C2), and 1.28×10^{-6} $(\Omega\ \text{cm})^{-1}$ (sample C3), respectively. The differences in electrical conductivity values of samples C2 and C3 correlate well with the XPS results.

TABLE 2. XRD and XPS investigation results: lattice parameter, a; particle size, D; binding energy, E_b; percentage of chemical state, %.

			XPS binding energy (eV)									
	(111) XRD		C 1s		Ag $3d_{5/2}$		O 1s		N 1s		Si 2p	
Sample	a (nm)	D (nm)	E_b (eV)	%	E_b (eV)	%	E_b (eV)	%	E_b (eV)	%	E_b (eV)	%
C1	0.4085	16	284.5	96	368.4	100	530.6	74	398.9	100	92.9	100
	0.4064	4	287.0	4			532.0	26				
C2	0.4082	9	282.5	32	367.7	39	530.5	47	398.0	68	100.5	11
	0.4034	3	284.5	68	369.6	59	532.0	53	399.3	32	102.5	81
C3	0.4065	5	282.6	27	367.5	55	530.0	65	397.4	52	100.7	78
			284.6	68	369.6	45	532.0	20	399.7	47	102.6	22
			286.5	5			533.3	15				

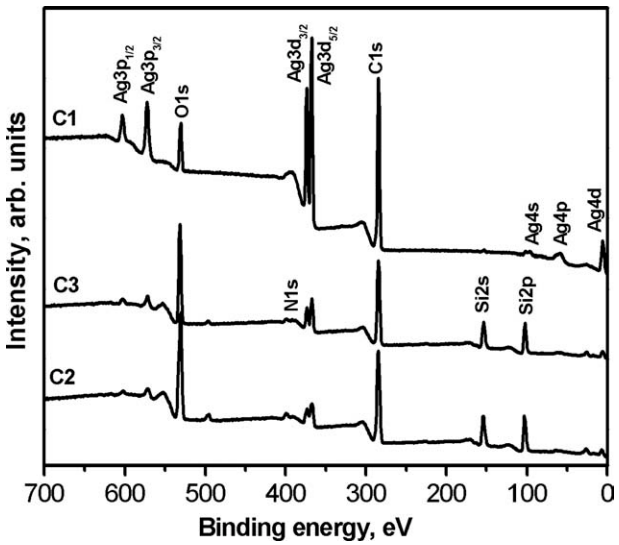

FIG. 2. XPS survey spectra of layered silicone-silver composites.

The plots *ln* (σ) vs. 1,000/T corresponding to samples C1, C2, and C3 are shown in Fig. 4. The conductivity of the investigated samples increases when the temperature increases, as would be expected for thermally activated conduction. In this case, the conductivity (σ) is expressed by the Arrhenius law by following equation,

$$\sigma = \sigma_0 \exp\left(-\frac{E_a}{k_B T}\right) \quad (1)$$

where σ_0 is a pre-exponential factor, E_a is thermal activation energy, and k_B is Boltzmann's constant. We first considered a least-square fit using *Eq. 1* in whole temperature range with the result shown in Fig. 4. At high temperatures ($T > 315$ K), *ln* σ shows a linear dependence with 1,000/T indicating that transport is dominated by a simple thermal activation process. On the other hand, there are deviations of the experimental curves from *Eq. 1* in the low temperature range ($T < 315$ K). This suggests that the electrical conduction in the films is not dominated by a simple thermal activation process at low temperatures. We consider that the variable range hopping conduction mechanism [16] may dominate at low temperatures.

We focus here on high temperature conductivity data of the samples. From the slopes and intercepts of the straight lines in Fig. 4, the values of the activation energy (E_a) and the pre-exponential factor (σ_0) are calculated for each sample. The inset in Fig. 4 presents the relationship between the E_a and the σ_0. The solid line indicates the best fit to the experimental data. We can clearly see that the experimental results can be well described by the MNR [17]. The MNR proposes a simple correlation between the E_a and the σ_0

$$\sigma_0 = \sigma_{00} \exp\left(\frac{E_a}{E_{MN}}\right) \quad (2)$$

where σ_{00} and $1/E_{MN}$ are the MNR prefactor and MNR slope, respectively [18]. The estimated σ_{00} and E_{MN} are 0.8 $(\Omega\ \text{cm})^{-1}$ and 44 meV, respectively, which are found

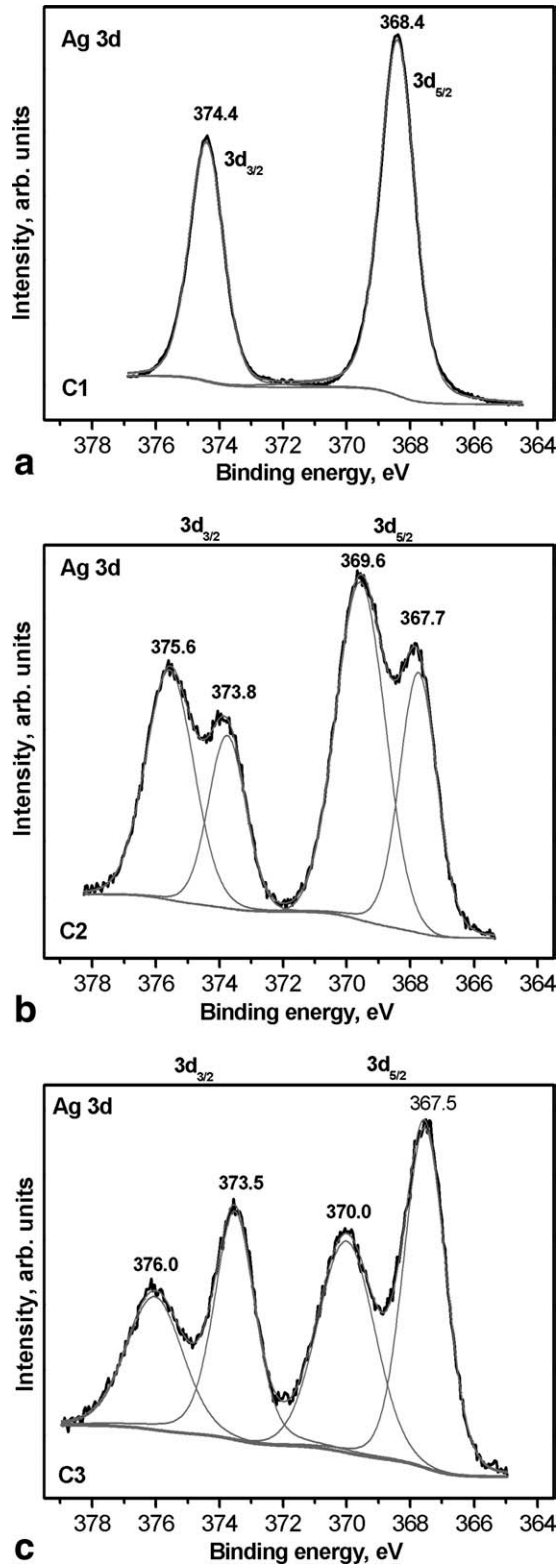

FIG. 3. Deconvolution of Ag 3d XPS spectra for the layered silicone-silver composites: (a) C1 (DMF solvent); (b) C2 (DMF+H_2O solvent); and (c) C3 (H_2O solvent).

DOI 10.1002/pc

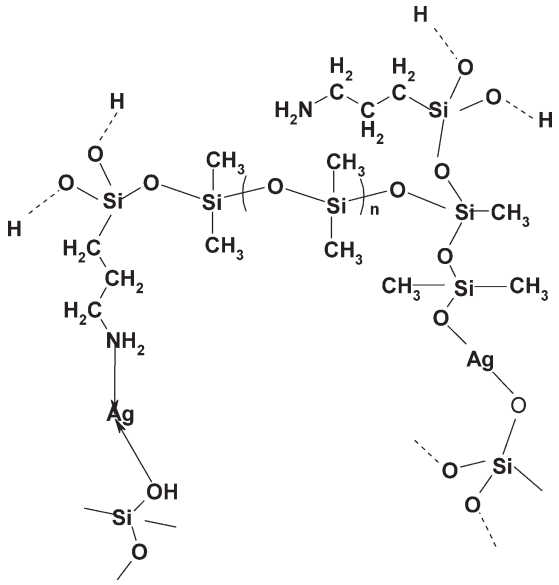

SCHEME 1. Possible locations of silver in silicone matrix.

to be typical for a variety of disordered materials [18]. Substituting *Eq. 2* into *Eq. 1* yields

$$\sigma = \sigma_{00}\exp\left[\left(\frac{1}{E_{MN}} - \frac{1}{k_B T}\right)E_a\right] \quad (3)$$

This gives a single crossing point for the different activation energies at a temperature (T_{MN}) given by

$$T_{MN} = \frac{E_{MN}}{k_B} \quad (4)$$

It is clearly that σ becomes independent on activation energy at this temperature. T_{MN} can be estimated from *Eq. 4* to be 515 K, which is very close to the experimental value (520 K) from Fig. 4. The MNR and experimental data are in excellent agreement.

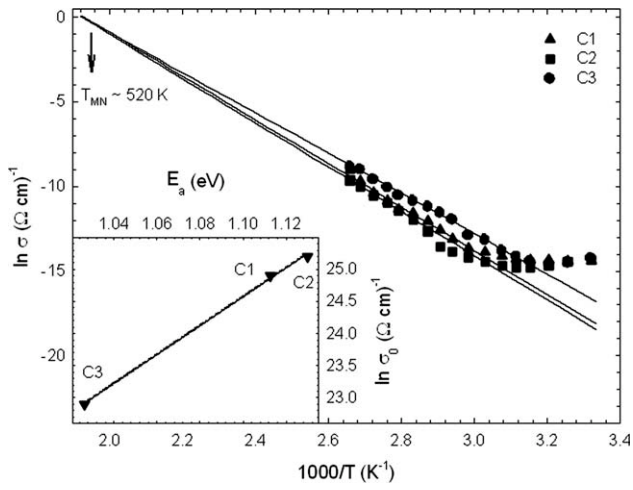

FIG. 4. Temperature dependence of the electrical conductivity plotted as *ln* (σ) vs. 1,000/*T* for the samples. Solid lines are the best-fit lines with *Eq. 1*. The inset of Fig. 4 represents the relationship between the pre-exponential factor (σ_0) and activation energy (E_a) at different stages of the preparing process. Solid line is the best-fit line with *Eq. 2*.

The applicability of the MNR to the conductivity data of the investigated samples in the high temperature region can be attributed to the statical shift of Fermi level which also accounts for the positive curvature of deviation in the Arrhenius plot of conductivity [19–22]. In this process, the conductivity is due to charge carriers at the mobility edge, so that E_a is the difference between the mobility edge and the Fermi level. A rather high value of σ_{00} also indicates that the observation of MNR in our case can be inferred in terms of the statical shift of the Fermi level with temperature, by assuming the conduction band tail with an exponential density of states distribution [20]. Therefore, we note that the MNR arises from the statical shift of Fermi level for the investigated samples.

CONCLUSION

Structural and electrical properties of some layered nanocomposites based on silicone matrix and silver particles have been investigated using XRD, XPS, and conductivity measurements.

XRD investigation evidenced a face-centered cubic structure for silver nanoparticles and a linear dependence of lattice parameter on the particle radius reciprocal. It was found that the (111) XRD peak can be decomposed in two Gaussian components with intensities dependent on DMF content in the reaction medium.

XPS studies indicate the migration of silver to the upper surface of the layer, when the synthesis mixture contained silver nitrate dissolved in DMF (sample C1). When silver nitrate was dissolved in water or in a mixture of water with DMF (sample C2 and sample C3), the binding energies are influenced by the effect of nanoparticle size, as well as by the disposal of Ag nanoparticles in different sites: ones that prevent and others that favor the oxidation process. Differences in the percentage of chemical states of Si 2p and C1s at the layer upper surface were also evidenced.

The room temperature electrical conductivity values and the temperature dependence of the electrical conductivity are dependent on the nanocomposite structure and homogeneity.

We found that the MNR can be applied to high temperature conductivity data of silicone-silver composites. We obtained that there is a strong correlation between the pre-exponential factor (σ_0) and activation energy (E_a). The origin of the MNR was attributed to the statical shift of Fermi level.

ACKNOWLEDGMENTS

The authors are thankful to B.F. Oprea for performing XPS measurements.

REFERENCES

1. Y.-J. Choi and T.J.M. Luo, *Appl. Mater. Interfaces*, **1**, 2778 (2009).
2. Y.-J. Choi, C.-K. Chiu, and T.-J.M. Luo, *Nanotechnology*, **22**, 045601 (2011).
3. Z. Li, A. Gu, and Q. Zhou, *Cryst. Res. Technol.*, **44**, 841 (2009).
4. A.S. Nair, N.P. Binoy, S. Ramakrishna, T.R.R. Kurup, L.W. Chan, C.H. Goh, M.R. Islam, T. Utschig, and T. Pradeep, *Appl. Mater. Interfaces*, **1**, 2413 (2009).
5. J.Y. Kim, M. Kim, H.M. Kim, J. Joo, and J.H. Choi, *Opt. Mater.*, **21**, 147 (2003).
6. Y.-J. Choi, U. Huh, and T.J.M. Luo, *J. Sol-Gel Sci. Technol.*, **51**, 124 (2009).
7. A.I. Amironesei, C. Tabacaru, I. Sandu, M. Cazacu, G.I. Rusu, and F. Iacomi, *Rev. Chim. (Bucharest)*, **62**, 455 (2011).
8. M. Cazacu, C. Racles, A. Airinei, A. Vlad, and I. Stoica, *Polym. Adv. Technol.* DOI: 10.102/pat. 1844.
9. W.H. Ki and M.P. Wang, *J. Nanopart. Res.*, **7**, 51 (2005).
10. W.J. Kim, M. Taya, and M.N. Nguyen, *Mech. Mater.*, **41**, 1116 (2009).
11. L.K. Neudachina, A.Ya. Golub, Yu.G. Yatluk, V.A. Osipova, Yu.A. Berdyugin, E.M. Gorbunov, L.V. Adamova, O.V. Koryakova, and M.V. Kuznetsov, *Inorg. Mater.*, **47**, 435 (2011).
12. R. Janardhanan, M. Karuppaiah, N. Hebalkar, and T.N. Rao, *Polyhedron*, **28**, 2522 (2009).
13. H.S. Shin, H.C. Choi, Y. Jung, S.B. Kim, H.J. Song, and H.J. Shin, *Chem. Phys. Lett.*, **383**, 418 (2004).
14. A. Babapour, O. Akhavan, R. Azimirad, and A.Z. Moshfegh, *Nanotechnology*, **17**, 763 (2006).
15. L.A. O'Hare, A. Hynes, and M.R. Alexander, *Surf. Interface Anal.*, **39**, 926 (2007).
16. N.F. Mott and E.A. Davis, *Electronic Processes in Non-Crystalline Materials*, Clarendon Press, Oxford (1971).
17. W. Meyer and H. Neldel, *Z. Tech. Phys.*, **12**, 588 (1937).
18. K. Shimakawa and F. Abdel-Wahab, *Appl. Phys. Lett.*, **70**, 652 (1997).
19. B.G. Yoon and C. Lee, *J. Appl. Phys.*, **60**, 673 (1980).
20. M.K. Rabinal and K.L. Narasimhan, *Philos. Mag. B*, **80**, 113 (2000).
21. H. Schmidt, M. Wiebe, B. Dittes, and M. Grundmann, *Appl. Phys. Lett.*, **91**, 232110 (2007).
22. I. Banik, *J. Ovonic Res.*, **7**, 15 (2011).